RNF213-associated urticarial lesions with hypercytokinemia

Camille Louvrier, Fawaz Awad, Anne Cosnes, Elma El Khouri, Eman Assrawi, Aphrodite Daskalopoulou, Bruno Copin, Hélène Bocquet, Sandra Chantot Bastaraud, Angela Arenas Garcia, et al.

RNF213-associated urticarial lesions with hypercytokinemia

Authors: Camille Louvrier PharmD PhD[1,2]*, Fawaz Awad MD PhD[1‡]*, Anne Cosnes MD[3]*, Elma El Khouri PhD[1], Eman Assrawi MD PhD[1], Aphrodite Daskalopoulou MSc[1], Bruno Copin MSc[1,2], Hélène Bocquet MD[3], Sandra Chantot Bastaraud MD[2], Angela Arenas Garcia MSc[1], Florence Dastot Le Moal PhD[2], Pierre De La Grange PhD[4], Philippe Duquesnoy MSc[1], Chiara I. Guerrera PhD[5], William Piterboth BSc[2], Nicolas Ortonne MD PhD[6], Olivier Chosidow MD PhD[3,7§], Sonia A. Karabina PhD[1§], Serge Amselem MD PhD[1,2]**, Irina Giurgea MD PhD[1,2]**

AFFILIATIONS

[1]Sorbonne Université, Inserm, Childhood Genetic Disorders, Hôpital Armand-Trousseau, 75012 Paris, France

[2]Département de Génétique Médicale, Assistance Publique–Hôpitaux de Paris (APHP), Hôpital Armand-Trousseau, 75012 Paris, France

[3]Faculté de Santé de Créteil et Service de Dermatologie, APHP, Hôpital Henri-Mondor, Université Paris-Est, 94000 Créteil, France

[4]GenoSplice, 75014 Paris, France

[5]Plateforme protéomique Necker, Université de Paris, Structure Fédérative de Recherche Necker, Inserm US24/CNRS UMS3633, 75015 Paris, France

[6]Département d'Anatomo-Pathologie, APHP, Hôpital Henri-Mondor, Créteil 94000, France

[7]Research Group Dynamic, EA7380, Faculté de Santé de Créteil, Ecole Nationale Vétérinaire d'Alfort, USC ANSES, Université Paris-Est Créteil, 94000 Créteil, France

[‡]Present address: Al-Quds University, Faculty of Medicine, Biochemistry and Molecular Biology Department; Abu Deis, Jerusalem, Palestine

*These authors contributed equally to this work.

[§]These authors contributed equally to this work.

**These authors contributed equally as co-last authors.

Correspondence to: Irina Giurgea and Serge Amselem, UMR_S933 Inserm, Sorbonne Université, Hôpital Armand Trousseau, 26, avenue du Dr. Arnold-Netter, 75012 Paris, France; Tel.: +33 1 44 73 52 39; Fax: +33 1 44 73 52 19; Email: irina.giurgea@inserm.fr; serge.amselem@inserm.fr

FUNDING

Institut National de la Santé et de la Recherche Médicale (INSERM) and Sorbonne University

Agence Nationale de la Recherche (ANR-17-CE17-0021-01)

H2020, European Union, Grant Agreement no. 779295 (SAK, SA)

INSERM “Poste d’accueil” program (00552404) (CL)

“Fondation pour la Recherche Médicale” (FDT20130928419) (FA)

French government grant (Ministère des Affaires Etrangères) (FA, EA)

Alquds University grant, Palestine (FA)

An-Najah University grant, Palestine (EA)

ABSTRACT

Background. Urticarial lesions are observed in both cutaneous and systemic disorders. Familial forms of urticarial syndromes are rare and can be encountered in systemic auto-inflammatory diseases.

Objective. We investigated a large family with dominantly inherited chronic urticarial lesions associated with hypercytokinemia.

Methods. We performed a genetic linkage analysis in 14 patients from a 5-generation family, as well as whole-exome sequencing, cytokine profiling and transcriptomic analyses on samples from two patients. The identified candidate protein was studied after *in vitro* expression of the corresponding normal and mutated recombinant proteins. An unsupervised proteomic approach was followed to unveil the associated protein network.

Results. The disease phenotype of the most affected family members is characterized by chronic urticarial flares associated with extremely high plasma levels of pro- (IL-1β, IL-6, TNF-α) and anti-inflammatory (IL-10, IL1-RA) cytokines, with no secondary organ dysfunction, no susceptibility to infections, no fever and normal C-reactive protein levels. Monocyte transcriptomic analyses identified an immunotolerant profile in the most affected patient. Affected family members carried a loss-of-function mutation in *RNF213* that encodes mysterin, a protein of poorly known physiological role. We identified the deubiquitinase CYLD, a major regulator of inflammation, as an RNF213 partner and showed that CYLD expression is inhibited by wild-type but not mutant RNF213.

Conclusion. We identified a new entity characterized by chronic urticarial lesions associated with a clinically-blunted hypercytokinemia. This disease, due to a loss of function of RNF213, reveals mysterin's key role in the complex molecular network of innate immunity.

KEY MESSAGES

- We describe a new disease entity, characterized by urticarial lesions that segregate as a fully penetrant autosomal-dominant trait associated with a chronic and clinically blunted hypercytokinemia.
- The obtained genetic and functional data reveal the critical role played by RNF213 in innate immunity.

CAPSULE SUMMARY

A germline mutation in *RNF213*, a new player in innate immunity encoding a protein called

mysterin, causes urticarial lesions associated with a clinically-blunted hypercytokinemia.

KEY WORDS

RNF213, hypercytokinemia, urticarial lesions, genetics

ABBREVIATIONS

CYLD: cylindromatosis

COVID-19: coronavirus-19 disease

CRP: C-reactive protein

DEG: differentially expressed genes

gnomAD: genome-aggregation database

HLA: human-leukocyte-antigen

IL: interleukin

IL-1RA: IL-1 receptor antagonist

IFN-γ: interferon-γ

LOD: logarithm of the odds

LPS: lipopolysaccharide

MHC II: major histocompatibility complex class II

MMD: moyamoya disease

RING: really interesting new gene

RNF213: ring-finger protein-213

SAIDs: systemic autoinflammatory diseases

SAA: serum amyloid A

TNF-α: tumor necrosis factor-α

WT: wild type

MAIN TEXT

Introduction

Urticaria is a common clinical condition characterized by the development of wheals and/or angioedema[1, 2]. Typical features of wheals include an itching sensation and a fleeting nature, the wheals lasting no more than 24 to 36 hours with no residual skin changes, whereas in its chronic form, the episodes last more than six weeks[1]. In addition, the patients with urticaria usually do not present with systemic symptoms.

In contrast to urticaria, the so-called "urticaria-like skin lesions" (or "urticarial skin lesions") are typically non-pruritic. They have a long duration, wheals are fixed, lasting several days or weeks and their resolution frequently leaves marks such as hyperpigmentation. In addition, systemic symptoms can coexist thereby defining systemic urticarial syndromes as is the case with disorders like urticarial vasculitis or like systemic autoinflammatory disorders (SAIDs), a group of rare heterogeneous diseases partly explained by mutations in genes that regulate the innate immune response[3]. In SAIDs, the recurrent episodes of systemic inflammation are driven by an excessive production of pro-inflammatory cytokines.

Herein, we report a genetic disease characterized by that, from a nosographic point of view, does not fall into any of the above-mentioned groups of diseases. Chronic urticarial lesions evolving by flares are the only clinical symptoms that segregate as a fully penetrant autosomal-dominant trait within a large family in which several affected members present persistent and massive −but extremely well-tolerated−hypercytokinemia. Genetic linkage analysis combined with whole-exome sequencing identified a disease-causing germline mutation in ring-finger protein-213 (*RNF213*), which encodes a protein called mysterin whose biological properties are still largely unknown. Unsupervised transcriptomic and proteomic approaches enabled exploration of *RNF213*-dependent biological pathways implicated in this new entity.

Methods

Patients

Clinical features were collected through a standardized form. The study conforms to the Helsinki declaration regarding ethical principles for medical research. Written informed consents were obtained from each patient or their parents.

Genetic studies

Genomic DNA samples were obtained from 16 family members.

Whole-genome genotyping of 14 family members (affected and healthy) used the Infinium Human Linkage-12 Genotyping BeadChip (Illumina). The BeadChip includes 6090 common single-nucleotide polymorphism markers with an average spacing of 441 kb and 0.58 centimorgan (cM) across the genome. Linkage analysis was performed with Merlin 1.1.2 software, assuming autosomal-dominant inheritance, full penetrance, no consanguinity and a mutation-allele frequency < 0.001.

Genomic DNA samples prepared from peripheral blood leukocytes of patients 1 (P1) and 2 (P2) were subjected to whole-exome sequencing, using the FlexiGene Kit (Qiagen). Exome-sequence libraries were prepared using a SeqCap EZ Human Exome Library Kit version 3.0 (Roche NimbleGen) and sequenced using a Nextseq500 (Illumina). The identified sequence variation was validated by Sanger sequencing on an ABI 3130 XL automated capillary DNA sequencer (Applied Biosystems).

Histological analysis

A skin punch biopsy was obtained from patient P1 under local anesthesia, then formalin-fixed and paraffin-embedded. Tissue sections (3-µm thick) were stained with hematoxylin, eosin and saffron and, after antigen retrieval by heat in appropriate buffer, immunolabeled with anti-CD3 (F.7.2.38 mouse monoclonal antibody, Dako), CD4 (4B12 monoclonal antibody, Leica), CD8 (C8/144B mouse monoclonal antibody, Dako), perforin (5B10 mouse monoclonal antibody, BioSB, Diagomics), granzyme B (11F1 mouse monoclonal antibody, Leica) and FOXP3 (236A/E7 mouse monoclonal antibody, Abcam) antibodies, using the Bond III device (Leica Microsystems).

RNF213 plasmid constructs and transfection

After reverse transcription, full-length *RNF213* cDNA underwent polymerase-chain reaction amplification (RT-PCR; Transcriptor High Fidelity cDNA Synthesis Kit, Roche) in two fragments of the *RNF213* transcripts. Each fragment was subcloned into pcDNA3.1/V5-His TOPO TA (Invitrogen). Each of the full-length *RNF213* cDNAs (WT and C41777R) was subsequently assembled into the pmaxGFP expression vector using the NEB builder Hifi DNA-Assembly Kit (New England BioLabs). Detailed method is provided in the **Suplemental data 1 in the Online Repository.**

HEK293T cells were transfected with different amounts of *RNF213* plasmids using FUGENE HD (Promega).

Cell-culture conditions

Monocytes were isolated from peripheral blood (EDTA-containing tubes) of P1, P2 and healthy donors provided by the Etablissement Français du Sang. For cytokine measurements, adherent monocytes were treated for 24 hours with 100 ng/ml lipopolysaccharide (LPS) and cell-culture supernatants were used for ELISA.

Dermal fibroblasts were isolated from skin biopsies obtained from P1, P2 and two healthy donors after obtaining their informed consent according to the Declaration of Helsinki.

Immortalized B lymphocytes were generated from three healthy donors' peripheral blood, at the Centre de Ressources Biologiques of Cochin Hospital (APHP, Paris).

HEK293T cells were maintained in standard conditions.

Detailed methods are provided in the **Supplemental data 1 in the Online Repository.**

Cytokine measurements

Patients' − P1, P2, P3 and P4 − and controls' plasma samples were prepared and stored immediately at –80°C, until analysis. Supernatants of adherent monocytes isolated from healthy controls' and patients' blood samples were centrifuged for 10 minutes at 250 *g* and stored at −80°C, until analysis. Cytokine concentrations were determined with ELISAs, according to the manufacturer's instructions (DuoSet ELISA kits, R&D, Biotechne).

Cell-lysate preparations

Cells (fibroblasts, immortalized B lymphocytes and HEK293T cells) were suspended in ice-cold lysis buffer (50 mM Tris, 100 mM NaCl, 5 mM EDTA, 1% Triton X–100, and phosphatase inhibitor (Roche Diagnostics) containing Complete Protease Inhibitor Cocktail (Roche Diagnostics). Lysates were incubated for 1 hour under agitation at 4°C and cleared by 10

minutes of centrifugation at 1000 *g*, 4°C.

Antibodies

Rabbit anti-human RNF213 polyclonal antibody (HPA003347, Sigma) was used for immunoprecipitation and immunoblot assays. Mouse anti-human cylindromatosis (CYLD) monoclonal antibody (sc-74434, Santa Cruz Biotechnology) and rabbit anti-human CYLD (D1A10) polyclonal antibody (8462S, Cell Signaling) were used for immunoblotting.

Immunoblotting

Cell lysates were loaded onto sodium dodecyl sulfate–polyacrylamide gel electrophoresis (SDS–PAGE) plates, transferred onto a PolyVinyliDene Fluoride (PVDF) or nitrocellulose membranes, blocked for 1 hour in PBS–Tween 0.1% (PBS-T)–5% skim milk and analyzed by Western-blotting with different antibodies, incubated overnight at 4°C in PBS-T–5% milk. The secondary antibody (rabbit– or mouse–horseradish peroxidase) was incubated for 1 hour at room temperature in PBS-T–5% milk. Proteins were detected with Amersham ECL Select Western-Blotting Detection Reagent (GE healthcare), according to the manufacturer's recommendations.

Cycloheximide (CHX) assay

HEK293T cells were transfected with RNF213_WT or RNF213_C4177R and treated with CHX (100 µg/ml) at different times during the 24 hours posttransfection, then washed with PBS and stored at –20°C until analysis.

Immunoprecipitation

Cell lysates (500 µl) of immortalized B cells and HEK293T cells were incubated overnight at 4°C with 2 µg of the anti-human RNF213 antibody. Cell lysates/antibody mixtures were then incubated with Pierce™ Protein G Magnetic Beads (ThermoFisher) for 1 hour at 4°C and washed five times with 500 µl of ice-cold lysis buffer, before being eluted after a 15-minute incubation with 40 µl of Leammli buffer.

Nanoscale liquid chromatography coupled to tandem mass spectrometry (NanoLC MS/MS) protein identification and quantification

Immunoprecipitation (IP) eluates were subjected to S-Trap™ micro-spin column digestion. Samples were injected into a nanoRSLC-Q Exactive PLUS (RSLC Ultimate 3000) (Thermo

Scientific). Peptides were loaded onto a µ-precolumn, and separated on a 50-cm reversed-phase liquid-chromatography column (Thermo Scientific). Peptides eluted from the column were analyzed by data-dependent MS/MS, using the top-10 acquisition method. Detailed method is provided in the **Supplemental data 1 in the Online Repository**.

NF-κB luciferase-reporter assay

HEK293T cells were co-transfected in 12-well plates with the following plasmids: 100 ng of *Firefly* luciferase-expression plasmid driven by NF-κB-responsive elements (pGL4.32, Promega), and 50 and 200 ng of pmaxGFP-vector or pRNF213-expression plasmids. Cells were lysed 40 hours posttransfection and subjected to luciferase-reporter assays (Promega) using a TriStar LB 941 Multimode Microplate Reader (Berthold Technologies).

Quantitative RT-PCR

Total RNA (1µg) from dermal fibroblasts was extracted using the RNeasy Mini Kit (Qiagen) and then subjected to reverse transcription with the Reverse Transcriptor Kit (Roche). The real-time PCR assays were performed in the Light Cycler LC480 (Roche). Detailed method is provided in the **Supplemental data 1 in the Online Repository.**

RNA-sequencing and transcriptomics analyses

mRNA-sequencing libraries (mRNA isolated from the monocytes of P1 and P2 and two healthy controls) were prepared with TruSeq Stranded mRNA kit (Illumina), according to supplier's recommendations and sequenced on paired-end 75 bp of Illumina HiSeq4000. Detailed method is provided in the **Supplemental data 1 in the Online Repository.**

RNA-Seq data are deposited at the National Center for Biotechnology Information in the Gene Expression Omnibus database (https://www.ncbi.nlm.nih.gov/geo/query/acc.cgi?acc=GSE168721, token: upahmkssptmfhcb).

Analysis of proteomics data

Results of RNF213 IP followed by nanoLC-MS/MS protein identification were analyzed with Perseus software. To avoid false-positive partners, only high-confidence interactions and specific interactions (interactors not detected with beads alone without IP) were retained.

Metascape (http://metascape.org)[4] was used on gene lists to analyze enrichment. That analysis included terms from Reactome Gene Sets, GO Biological Processes, and KEGG Pathways.

Statistical analyses

Differences were analyzed using unpaired Student *t*-tests and were plotted with Prism 9, GraphPad software, (San Diego, CA). A P value ≤ 0.05 defined statistical significance.

Results

Disease phenotype

We studied a multiplex family with urticarial lesions segregating as an autosomal-dominant trait (**Figure 1A**). Affected family members had early-onset episodes (age 6 months to 25 years) of nonpruritic fixed urticarial lesions characterized by erythematous and edematous hives spontaneously resolving after several weeks into large violaceous macules that fade over time, but persist over months or years (**Figure 1B**). These cutaneous lesions displayed an episodic course and were triggered by seasonal temperature variations; the patients spontaneously reported an exacerbation of their cutaneous symptoms after a drop in ambient temperature. However, all the ice cube tests performed in one of the patients (Patient 1) remained negative.

Patient 1 (P1), now a 55-year-old woman, first consulted in our dermatology department in 1987, because of the occurrence since the age of 12 of erythematous, nonpruritic, urticarial lesions on her ankles. Over the years, as the flares became more frequent, cutaneous lesions extended over the trunk, arms, legs and face. During her 35-year follow-up, she never experienced any other symptoms: especially no fever, arthralgias or angioedema. Histological examination of P1's biopsied lesional skin revealed minor inflammatory infiltrates in the upper dermis, interspersed with uninvolved, normal epidermis. Infiltrates were comprised of small lymphocytes admixed with few neutrophils and scattered nuclear debris, without vasculitis (**Figure E1 in the Online Repository**). The investigations performed over the years documented chronic lymphopenia (0.4 to 0.6 G/l), with markedly low CD4+ T cells (167 cells/µl) and modestly low CD8+ T cells (167 cells/µl) (see **Figure E2.A in the Online Repository**) and, sometimes, antinuclear antibody-positivity (titers range 80 to 1280, with no other autoantibodies). Conventional inflammatory parameters, e.g., Plasma C-reactive protein (CRP) and serum amyloid A (SAA) levels were within normal and in subnormal ranges, respectively. Complement system tests (total complement activity, C3 and C4) were also within normal ranges (see **Figure E2.A in the Online Repository**). Serum-protein electrophoresis showed mild polyclonal gammopathy with no monoclonal gammopathy. Although no definite diagnosis could be made, and because of the psycho-social burden experienced by P1, several treatment lines, e.g., antihistamines, hydroxychloroquine, methotrexate, thalidomide, dapsone or colchicine, were tried but had no efficacy. More targeted treatment such as anakinra or adalimumab were prescribed, each for 3 to 6 months with no regression of the cutaneous lesions. Prednisone 20 mg/day or topical clobetasol propionate 0.05% (20 g/day) provided partial lesion attenuation but was difficult to sustain over the long-term.

Patient 2 (P2) is a 56-year-old woman who first consulted in our department in 1987 because of skin lesions, similar to those of her sister P1, and localized on arms and buttocks. The lesions appeared when she was 1-year old but did not extend over the years. During her 34-year follow-up, she did not complain of any other symptoms. Like her sister, no biological inflammation was observed (see **Figure E2.A in the Online Repository**). Topical clobetasol propionate 0.05% (20 g/week) provided partial lesion attenuation.

Other affected family members: Nine other family members exhibiting the same cutaneous lesions were identified (**Figure 1C)**. All of them had early-onset episodes (from the age of 6 months to 25 years). The lesions were similar to those of P1 and P2. None of the patients reported other symptoms, fever, arthralgias or angioedema. Furthermore, they never had serious infections. Routine biological tests performed in 4 of these patients are provided in **Figure E2.A in the Online Repository**.

Notably, a large intrafamilial contamination with COVID-19 (confirmed by SARS-Cov-2 Real-time PCR test assay) occurred in 2020. None of the family members was vaccinated at that time. P1 had transitory anosmia, headaches and odynophagia, and her 87-year-old mother, transient fever and fatigue. The other affected family members were asymptomatic.

Massive hypercytokinemia and monocyte immunosuppression

P1's and P2's plasma inflammatory cytokine levels were determined at different times over 3 years. Plasma levels of proinflammatory (e.g., interleukin (IL)-1β, IL-6, IL-1α, IL-8 and tumor necrosis factor-α (TNF-α)) and anti-inflammatory mediators (like IL-1 receptor-antagonist (IL1-RA) and IL-10) were extremely elevated, P1 having higher plasma levels of all cytokines (**Figure 2A**). Moreover, P1 had high levels of the Th2-type cytokine IL-4, while P2's IL-4 was below the detection limit. Conversely, P1's and P2's Th1-type cytokines IL-12 and interferon-γ (IFN-γ) were comparable to those of healthy controls (**Figure 2A**). Levels of all these cytokines remained constant over time, even when P1 received anti-TNF (adalimumab) or anti-IL1 (anakinra) agents. We also measured, in the same assay; the plasma cytokine levels (i.e., IL-1β, TNF-α, IL-6 and IL-10) of P1 and P2 together with two additional patients from this family (P3 and P4) (see **Figure E2.B in the Online Repository**). This analysis revealed that the hypercytokinemia of P1 and P4—the patients with the most severe skin lesions—was massive, whereas, P3, had cytokine levels within the normal range.

Furthermore, we studied cytokine secretion in the supernatants of monocytes isolated from P1, P2 and healthy donors, before and after lipopolysaccharide (LPS) stimulation. Notably,

after LPS stimulation, P1's and P2's IL-1β levels were significantly lower in their monocyte supernatants than in those of healthy controls, while the other cytokines tested (TNF-α, IL-6 and IL-18) did not differ significantly (**Figure 2B**). Additionally, the amount of IL-6 in the supernatants of cultured skin fibroblasts isolated from P1 and P2 was similar to that of healthy donors (see **Figure E2.C in the Online Repository**).

In an attempt to identify a possible dysregulation of the gene networks associated with this massive hypercytokinemia, monocytes from P1, P2 and two healthy controls were subjected to transcriptomic analysis (RNA-Seq). Differentially expressed genes (DEGs) were analyzed between each patient and mean healthy control values (i.e., DEGs with $P \leq 0.05$ and a |fold change| $\geq$1.5). That analysis showed that P1's gene-expression dysregulation was more pronounced than P2's (2,011 and 675 DEGs, respectively, see **Table E1.A** and **E1.B in the Online Repository**), in keeping with the severity of their disease phenotypes. The significantly upregulated gene set was enriched in several pathways, such as: "positive regulation of cell migration" (GO:0030335), "myeloid leukocyte activation" (GO:0002274) and "response to bacterium" (GO:0003617) (**Figure 2C**, see **Figure E3.A, Table E1.C** and **E1.D in the Online Repository**), and mainly concerned P1 who has a more severe disease. Notably, eight of P1's top-20 upregulated genes (*OLFM4*, *RETN*, *BPI*, *LCN2*, *LTF*, *CAMP*, *MMP8* and *ARG1*) are overexpressed during sepsis[5-9] (see **Figure E3.B in the Online Repository**), with *ARG1* being considered a potential mediator of sepsis-induced immunosuppression[8].

To further investigate the relationships between P1's transcriptomic profile and that of patients with sepsis (i.e., patients with prominent hypercytokinemia), we took advantage of available transcriptomic datasets (GSE133822) from the monocytes of 33 patients with sepsis[8]. While relying on the list of P1's DEGs, we computed Pearson's correlation coefficients (using fold-change values) between P1, P2 or each of the 33 septic patients versus healthy samples from the same dataset, and between each of the 33 septic patients (**Figure 2D**). A strong correlation was found between P1's transcriptomic data and that of each septic patient, similar to what was found between each of the 33 septic patients (respective mean coefficient correlations of 0.36 and 0.42, see **Table E1.E in the Online Repository**). Among the set of downregulated genes (see **Figure E3.C**, **Table E1.F** and **E1.G in the Online Repository**), P1's human-leukocyte–antigen (HLA) transcripts encoding the cell-surface receptors of major histocompatibility complex class II (MHC II), including HLA-DR, were downregulated (**Figure 2E**); such HLA-DR downregulation is a known biomarker of monocyte immunosuppression[10].

Identification of a pathogenic mutation in RNF213

To determine the molecular basis of this condition that segregates as an autosomal-dominant trait (**Figure 1A**) with complete penetrance and variable expressivity, genetic linkage analysis was done on 14 family members. A significant logarithm of the odds (LOD) score was identified for a single 3.3-Mb region of chromosome 17 (chr17:76141133–79461642; hg19 genome assembly) (see **Figure E4.A in the Online Repository**). Whole-exome sequencing of P1 and P2 identified a single variation absent from the genome-aggregation database (gnomAD): c.12529T>C p.(Cys4177Arg) in *RNF213*, a large gene that contains 68 exons (see **Figures E4.B to E4.D in the Online Repository** and **Figure 3A**). As expected from the genetic linkage data, this missense variation perfectly segregates with the phenotypic status of all 16 family members tested (**Figure 1A**). The RNF213 protein (also known as mysterin) is a large, ubiquitously expressed 5207-amino-acid protein. It comprises an AAA core with ATPase activity and an E3 module harboring a RING (really interesting new gene)-finger domain with E3 ubiquitin-ligase activity[11]. The identified sequence variation leads to amino-acid substitution at codon 4177 involving a cysteine, invariant throughout evolution and located within the E3 module (**Figure 3A**). Taken together, these data strongly suggest that the c.12529T>C p.(Cys4177Arg) missense variation identified in *RNF213* is causative in this family.

To further confirm this hypothesis, we first assessed the potential impact of the identified missense variation on RNF213 transcripts and proteins isolated from the patients' dermal fibroblasts (two independent skin biopsies (P1- and P2SB1, and P1- and P2SB2) for each patient). *RNF213*-mRNA expression did not differ between patients' fibroblasts and those of controls (see **Figure E5.A in the Online Repository**). However, RNF213-protein levels were significantly lower in both patients' fibroblasts, suggesting that the p.(Cys4177Arg) variation affected RNF213 half-life (**Figure 3B** and **see Figure E5.B in the Online Repository**).

After subcloning the full-length 15-kb *RNF213* cDNA in a eukaryotic expression vector, RNF213 stability was examined in HEK293T cells expressing recombinant forms of the protein carrying the p.(Cys4177Arg) variation or not (i.e., RNF213_C4177R or wild-type RNF213_WT, respectively). The experimental results revealed a shorter half-life RNF213_C4177R as compared to its WT counterpart (4 vs. 6.5 hours, $P = 0.0234$; **Figure 3C**, see **Figure E5.C in the Online Repository**), a result supporting that the p.(Cys4177Arg) variation is a loss-of-function mutation.

Taking advantage of the recent finding suggesting that RNF213 is a positive regulator of NF-κB signaling[12, 13], we used an NF-κB-dependent luciferase-reporter assay to assess the impact of the identified mutation on that signaling activity (**Figure 3D**). As expected,

HEK293T cells transfected with the expression plasmid encoding RNF213_WT displayed enhanced NF-κB activity, compared to mock-transfected cells; however, cells expressing RNF213_C4177R had completely lost NF-κB activation.

Taken together, these observations demonstrate RNF213 involvement in the pathogenesis of family's disease phenotype.

RNF213 role in inflammation

To further investigate the molecular mechanism underlying this disease condition and gain additional insight into the RNF213-dependent biological pathways, we used an unsupervised proteomic approach to identify cell-protein partners interacting with RNF213. To do so, we immunoprecipitated RNF213 from two different cell types—immortalized B cells (from three healthy controls) and native HEK293T cells—followed by nanoLC-MS/MS protein identification and quantification. That analysis identified 104 RNF213 interactors, 64 in immortalized B cells and 60 in HEK293T cells, with 20 shared by B cells and HEK293T cells (see **Figure E6.A**, **Table E2.A** and **E2.B in the Online Repository**), thereby confirming the robustness of the approach used.

Protein-enrichment analysis revealed RNF213-associated biological pathways, several of which agree well with the patients' hypercytokinemia, i.e., "cytokine-mediated signaling pathways" (GO:0019221), and with innate immunity, i.e., "budding and maturation of HIV virions" (R-HSA-162588), and "positive regulation of viral release from host cells" (GO:1902188) (**Figure 4A**, and see **Table E2.C** and **E2.D in the Online Repository**). Notably, the proteins involved in the cytokine-mediated signaling pathway include well-known immunity regulators, such as CYLD, ISG15, OAS2 and ISG20. Among them, CYLD (cylindromatosis), detected in both cell types, is a deubiquitinase that negatively regulates the NF-κB pathway[14]. The RNF213–CYLD interaction was confirmed in HEK293T by co-immunoprecipitation followed by western-blot analysis (see **Figure E5.B in the Online Repository**).

We subsequently tested the impact of RNF213 on CYLD expression, to determine whether the latter could represent a functional link between RNF213 and the NF-κB pathway. To this end, HEK293T cells were transfected with the RNF213_WT- or RNF213_C4177R-encoding constructs (**Figure 4C**). RNF213_WT-expressing cells expressed significantly less CYLD protein than mock-transfected cells, and that lower expression was partially lost when cells were transfected with mutated *RNF213* (**Figure 4C**). These CYLD-expression results are

consistent with the effects of RNF213_WT and RNF213_C4177R that we observed on NF-κB activation (**Figure 3D**).

Discussion

Herein, we describe a novel entity characterized by the association of urticarial lesions with chronic and massive —but well-tolerated—hypercytokinemia. We provide genetic and molecular evidence supporting that this disease, which is a genetic condition segregating as a fully penetrant trait with variable expressivity, is due to a germline mutation in *RNF213*. Additional functional studies based on unsupervised approaches identified the key role played by mysterin—the *RNF213*-encoded protein—in the complex network of proteins involved in innate immunity.

From a nosographic viewpoint, it is important to underline the fact that the skin lesions of this family, although ressembling urticaria, differ from urticaria in that they are non-pruritic and fixed, spontaneously resolving in pigmented scares that fade over time. Moreover, unlike what is observed in SAIDs, the patients from this family have never reported any inflammatory systemic symptom (while P1 and P2 have been followed twice a year for more than 30 years). Furthermore, in spite of the absence of systemic symptoms, several patients have extremely high plasma cytokine levels.

The hypercytokinemia identified in P1 and P2 from this family is not an acute phenomenon but persists in a chronic state, as documented by the patients' long-term follow-up. In P1, the most severely affected, several proinflammatory cytokine levels (e.g., IL-1β, TNF-α or IL-6) were much higher than those found in patients with an acute cytokine storm requiring intensive care, as seen in patients with severe sepsis[15] or COVID-19[16, 17]. Paradoxically, in our patients, the disease is extremely well-tolerated, without any organ dysfunction or general symptoms. The patients remained apyretic and plasma levels of common biological markers of systemic inflammation (e.g., CRP) were within normal ranges.

In an attempt to at least partly explain this clinical–biological dissociation, additional biological assays were undertaken. Indeed, the proinflammatory phenotype was associated with high plasma levels of IL-1–receptor antagonist and IL-10, two markers of an anti-inflammatory response. Transcriptomic analyses revealed an immunosuppressive phenotype of P1's monocytes, including less expression of MHC class II transcripts, thereby mimicking sepsis-induced immunosuppression. Pertinently, severe COVID-19 patients also exhibit these features[14, 15].

P1's chronic lymphopenia is another element shared with septic patients in whom lymphopenia is a well-known phenomenon attributed to apoptosis[18]. In this context, it is worth noting that apoptosis contributes to sepsis-induced immunosuppression[10] through the immune tolerance induced by IL-10 secretion[6] and the shift of the Th1/Th2 balance towards Th2 cells[19]. P1's cytokine profile clearly favors this Th2 profile, with high plasma IL-4 and IL-10 concentrations associated with IFN-γ and IL-12 levels below the limit of detection. In contrast to patients with sepsis-induced cytokine storms, our patients had no heightened susceptibility to infections known to occur in acquired immunosuppression. As just recently noted, the putative impact of inborn errors in *RNF213* on adaptative immune responses is so far unknown[20]. The fact that our patients have no heightened susceptibility to infections provides a first answer to that question.

This disease, which is caused by a germline pathogenic *RNF213* mutation, is so far revealed by the study of a single family. Identification of additional families with inborn errors of *RNF213* associated with immune dysregulation would be of great help to better characterize this new disease entity. It should, however, be noted that the current data rely on the study of a five-generation family with more than 10 affected patients, the in-depth phenotyping of two of these patients through ~35 years of longitudinal follow-up, and a genetic strategy based on two unsupervised approaches (i.e., whole-genome linkage analysis with a LOD score >3 and whole exome sequencing). In addition, the results of different functional tests (i.e., CHX and NF-κB luciferase-reporter assays) confirmed that the sequence variation identified in *RNF213* is disease-causing. Notably, other *RNF213* sequence variations have been associated with moyamoya disease (MMD), a rare cerebral angiopathy characterized by progressive stenosis of the intracranial and internal carotid arteries, engendering ischemic and hemorrhagic stroke[21, 22]. In MMD, some *RNF213* variants, which are low-penetrant variants, are commonly considered genetic-susceptibility factors, suggesting that additional factors are required to develop the disease. In this setting, the identification of over 100 new RNF213-protein partners is valuable information that could contribute greatly to further deciphering MMD pathophysiology. Recently, two patients with a severe syndromic form of moyamoya disease (MMD) including skin involvement and *de novo* RNF213 missense variations have been reported in a clinical report[23]. Notably, for one of the two patients, the description of the skin lesions recalls the urticarial lesions observed in our family. Although no studies were performed to assess the functional consequences of the identified *RNF213* missense variations, the possibility that the disease of our family and of these two sporadic cases belong to the same nosological entity remains open.

In our study, RNF213 emerges as a new innate-immunity actor playing a key role in inflammation. That finding agrees with very recent results emphasizing RNF213's role during bacterial and viral infection[20, 24, 25]. Our analyses identified CYLD, an RNF213 cell-protein partner, as a potential missing link accounting for the ability of RNF213 to activate the NF-κB pathway. As demonstrated herein, RNF213 inhibited CYLD expression and, accordingly, the mutated RNF213 carrying the p.(Cys4177Arg) loss-of-function mutation failed to inhibit CYLD expression. Most importantly, CYLD deubiquitinase, which is known to inhibit the NF-κB pathway, activates cell death[14]. And as shown in the mouse, such cell death, in turn, drives severe skin inflammation[26]. It is therefore tempting to speculate that the impaired CYLD suppression observed in the context of RNF213_C4177R is at least in part responsible for our patients' skin condition. Notably, a similar NF-κB blockade has already been described in genetic diseases with skin inflammation such as those due to loss-of-function mutations in *IKBKG* (the gene encoding NEMO, a substrate of CYLD)[27], in *RELA* (the gene encoding p65, a NF-κB subunit)[28] or in *CARD14*[29].

In summary, we describe a disease entity, characterized by urticarial lesions that segregate as a fully penetrant autosomal-dominant trait associated with a chronic, massive and clinically blunted hypercytokinemia. The genetic and functional data obtained during the course of this study, which reveal the critical role RNF213 played in innate immunity, should open new avenues for identifying novel insights in the regulation of the immune system. Identification of additional families with inborn errors of *RNF213* associated with immune dysregulation should help to better characterize this new disease entity and, therefore, identify an effective therapy.

ACKNOWLEDGMENTS

We are grateful to the patients and their family, whose cooperation made this study possible and Prof. Laurence Fardet for her contribution to clinical data acquisition. We also would like to thank Janet Jacobson for editing the manuscript.

REFERENCES

1. Zuberbier T, Aberer W, Asero R, Abdul Latiff AH, Baker D, Ballmer-Weber B, et al. The EAACI/GA(2)LEN/EDF/WAO guideline for the definition, classification, diagnosis and management of urticaria. Allergy 2018; 73:1393-414.
2. Peroni A, Colato C, Schena D, Girolomoni G. Urticarial lesions: if not urticaria, what else? The differential diagnosis of urticaria: part I. Cutaneous diseases J Am Acad Dermatol 2010; 62:541-55.
3. Manthiram K, Zhou Q, Aksentijevich I, Kastner DL. The monogenic autoinflammatory diseases define new pathways in human innate immunity and inflammation. Nat Immunol 2017; 18:832-42.
4. Zhou Y, Zhou B, Pache L, Chang M, Khodabakhshi AH, Tanaseichuk O, et al. Metascape provides a biologist-oriented resource for the analysis of systems-level datasets. Nat Commun 2019; 10:1523.
5. Almansa R, Ortega A, Avila-Alonso A, Heredia-Rodriguez M, Martin S, Benavides D, et al. Quantification of Immune Dysregulation by Next-generation Polymerase Chain Reaction to Improve Sepsis Diagnosis in Surgical Patients. Ann Surg 2019; 269:545-53.
6. Cohen G, Ilic D, Raupachova J, Horl WH. Resistin inhibits essential functions of polymorphonuclear leukocytes. J Immunol 2008; 181:3761-8.
7. Martin L, van Meegern A, Doemming S, Schuerholz T. Antimicrobial Peptides in Human Sepsis. Front Immunol 2015; 6:404.
8. Washburn ML, Wang Z, Walton AH, Goedegebuure SP, Figueroa DJ, Van Horn S, et al. T Cell- and Monocyte-Specific RNA-Sequencing Analysis in Septic and Nonseptic Critically Ill Patients and in Patients with Cancer. J Immunol 2019; 203:1897-908.
9. Hu Z, Murakami T, Suzuki K, Tamura H, Reich J, Kuwahara-Arai K, et al. Antimicrobial cathelicidin peptide LL-37 inhibits the pyroptosis of macrophages and improves the survival of polybacterial septic mice. Int Immunol 2016; 28:245-53.
10. Venet F, Demaret J, Gossez M, Monneret G. Myeloid cells in sepsis-acquired immunodeficiency. Ann N Y Acad Sci 2020.
11. Ahel J, Lehner A, Vogel A, Schleiffer A, Meinhart A, Haselbach D, et al. Moyamoya disease factor RNF213 is a giant E3 ligase with a dynein-like core and a distinct ubiquitin-transfer mechanism. Elife 2020; 9.
12. Piccolis M, Bond LM, Kampmann M, Pulimeno P, Chitraju C, Jayson CBK, et al. Probing the Global Cellular Responses to Lipotoxicity Caused by Saturated Fatty Acids. Mol Cell 2019; 74:32-44 e8.

13. Takeda M, Tezuka T, Kim M, Choi J, Oichi Y, Kobayashi H, et al. Moyamoya disease patient mutations in the RING domain of RNF213 reduce its ubiquitin ligase activity and enhance NFkappaB activation and apoptosis in an AAA+ domain-dependent manner. Biochem Biophys Res Commun 2020; 525:668-74.

14. Lork M, Verhelst K, Beyaert R. CYLD, A20 and OTULIN deubiquitinases in NF-kappaB signaling and cell death: so similar, yet so different. Cell Death Differ 2017; 24:1172-83.

15. Gogos CA, Drosou E, Bassaris HP, Skoutelis A. Pro- versus anti-inflammatory cytokine profile in patients with severe sepsis: a marker for prognosis and future therapeutic options. J Infect Dis 2000; 181:176-80.

16. Wang SY, Takahashi T, Pine AB, Damsky WE, Simonov M, Zhang Y, et al. Challenges in interpreting cytokine data in COVID-19 affect patient care and management. PLoS Biol 2021; 19:e3001373.

17. Giamarellos-Bourboulis EJ, Netea MG, Rovina N, Akinosoglou K, Antoniadou A, Antonakos N, et al. Complex Immune Dysregulation in COVID-19 Patients with Severe Respiratory Failure. Cell Host Microbe 2020; 27:992-1000 e3.

18. Hotchkiss RS, Monneret G, Payen D. Sepsis-induced immunosuppression: from cellular dysfunctions to immunotherapy. Nat Rev Immunol 2013; 13:862-74.

19. Girkontaite I, Urbonaviciute V, Maseda D, Neubert K, Herrmann M, Voll RE. Apoptotic cells selectively suppress the Th1 cytokine interferon gamma in stimulated human peripheral blood mononuclear cells and shift the Th1/Th2 balance towards Th2. Autoimmunity 2007; 40:327-30.

20. Thery F, Martina L, Asselman C, Zhang Y, Vessely M, Repo H, et al. Ring finger protein 213 assembles into a sensor for ISGylated proteins with antimicrobial activity. Nat Commun 2021; 12:5772.

21. Kamada F, Aoki Y, Narisawa A, Abe Y, Komatsuzaki S, Kikuchi A, et al. A genome-wide association study identifies RNF213 as the first Moyamoya disease gene. J Hum Genet 2011; 56:34-40.

22. Liu W, Morito D, Takashima S, Mineharu Y, Kobayashi H, Hitomi T, et al. Identification of RNF213 as a susceptibility gene for moyamoya disease and its possible role in vascular development. PLoS One 2011; 6:e22542.

23. Strong A, O'Grady G, Shih E, Bishop JR, Loomes K, Diamond T, et al. A new syndrome of moyamoya disease, kidney dysplasia, aminotransferase elevation, and skin disease associated with de novo variants in RNF213. American Journal of Medical Genetics Part A 2021; 185:2168-74.

24. Otten EG, Werner E, Crespillo-Casado A, Boyle KB, Dharamdasani V, Pathe C, et al. Ubiquitylation of lipopolysaccharide by RNF213 during bacterial infection. Nature 2021.

25. Houzelstein D, Simon-Chazottes D, Batista L, Tokuda S, Langa Vives F, Flamand M, et al. The ring finger protein 213 gene (Rnf213) contributes to Rift Valley fever resistance in mice. Mamm Genome 2021; 32:30-7.

26. Kumari S, Van TM, Preukschat D, Schuenke H, Basic M, Bleich A, et al. NF-kappa B inhibition in keratinocytes causes RIPK1-mediated necroptosis and skin inflammation. Life Science Alliance 2021; 4.

27. Smahi A, Courtois G, Vabres P, Yamaoka S, Heuertz S, Munnich A, et al. Genomic rearrangement in NEMO impairs NF-kappaB activation and is a cause of incontinentia pigmenti. The International Incontinentia Pigmenti (IP) Consortium. Nature 2000; 405:466-72.

28. Badran YR, Dedeoglu F, Castillo JML, Bainter W, Ohsumi TK, Bousvaros A, et al. Human RELA haploinsufficiency results in autosomal-dominant chronic mucocutaneous ulceration. Journal of Experimental Medicine 2017; 214:1937-47.

29. Peled A, Sarig O, Sun GP, Samuelov L, Ma CA, Zhang Y, et al. Loss-of-function mutations in caspase recruitment domain-containing protein 14 (CARD14) are associated with a severe variant of atopic dermatitis. Journal of Allergy and Clinical Immunology 2019; 143:173-+.

CONFLICT OF INTEREST

The authors have no conflict of interest to declare.

FIGURE LEGENDS

Figure 1. Genealogical tree of the studied family and clinical manifestations in affected members. (**A**) Genealogical family tree showing co-segregation of chronic urticarial lesions (filled symbols) with the identified *RNF213* pathogenic variation. †, died (**B**) Patient 1's (P1) and 2's (P2) urticarial lesions. N: normal allele, M: mutated allele. (**C)** Clinical characteristics of affected family members.

Figure 2. Hypercytokinemia and monocyte immunosuppression. (**A**) ELISA-assessed plasma-cytokine levels of patients P1 and P2 (over 3 years) and 9–10 healthy donors (Ctr). **(B**) Cytokines (ELISA) in the supernatants of P1's (n = 4) and P2's (n = 4) and 5–6 healthy controls' untreated or lipopolysaccharide (LPS)-stimulated monocytes. **A** & **B**: means ± standard deviation. (**C–E**) RNA-Seq analyses of patients' monocytes expressed as fold changes (FC) compared to the mean Ctr value. (**C**) Heatmap of enriched terms across the list of patients' up-regulated genes, colored by *P*-values. (**D**) Heatmap of Pearson's correlation coefficients using patients' RNA-Seq data and 33 septic patients' monocyte transcriptomic datasets (GSE133822)[5]. Based on P1's list differently expressed genes (DEGs, $|FC| > 1.5$, $P < 0.05$), Pearson's correlation coefficients (FC values) were calculated between P1 or P2 and each of the 33 septic patients and between each of the 33 septic patients (mean correlation coefficients = 0.36, 0.05 and 0.42, respectively). (**E**) |FCs| of P1's and P2's HLA mRNAs encoding major histocompatibility complex class II (MHCII). Underlined DEG values are significant (> 1.5, $P < 0.05$). Two-tailed *P* values were determined with unpaired *t*-tests. ns: not significant; *$P \leq 0.05$; **$P \leq 0.01$; ***$P \leq 0.001$.

Figure 3. *RNF213* p.(Cys4177Arg) mutation: identification and functional assessment. (**A**) Top left: *RNF213*-gene schematic representation (exons (black), mutation-containing exon-47 (red)) and domain-organization model of the corresponding protein, showing the identified mutation. CTD, C-terminal domain. Top right: Sanger electrophoregram showing the heterozygous *RNF213* mutation c.12529T>C, p.(Cys4177Arg) (arrow). Bottom left: Evolutionary conservation of RNF213-protein amino-acid Cys4177 in different species. Bottom right: 3D structure of mouse rnf213 (6TAX in the Protein Data Bank) Cys4171 corresponding to human-RNF213 Cys4177 in red. The E3 module includes: back (orange), RING (green), shell (yellow) and core (light yellow) subdomains. (**B**) RNF213-protein quantification in patient 1's (P1) and 2's (P2) dermal fibroblasts (independent skin biopsies

(SB1) and (SB2)) and two healthy controls. (**C**) Cycloheximide-assay assessment of *RNF213* p.(Cys4177Arg)-mutation impact on protein stability after transient mutated-protein expression in HEK293T cells ($P = 0.023$). (**D**) *RNF213*-mutation impact on NF-κB activity. HEK293T cells were transfected with 50 or 200 ng of the WT or C4177R-mutant RNF213 constructs or the pmaxGFP construct (mock) as control, and an NF-κB reporter construct (100 ng). (**B, C, D**) Two-tailed *P* values were determined in unpaired *t*-tests of means ± SD. ns: not significant; *$P \leq 0.05$; ***$P \leq 0.001$.

Figure 4. Signaling pathways inferred from networks of proteins interacting with RNF213. (A) Immunoprecipitation-assay identification of RNF213 partners in immortalized B cells and native HEK293T cells followed by NanoLC MS/MS. Proteins are grouped into clusters based on their similarities (networks of enriched terms are represented as pie charts, with pies color-coded based on cell type (red: HEK293T cells, blue: immortalized B cells); pie size is proportional to the total number of hits that fall into that specific term). Edge thickness between nodes represents the number of RNF213-interacting proteins shared by both pathways. Colored halos, which regroup closely related pathways, include the "cytokine-mediated signaling pathway" highlighted in bold. (**B**) List of protein partners of RNF213 identified under the enriched term "Cytokine-mediated signaling pathway". Red: HEK293T cells; blue: immortalized B cells. **C.** CYLD-protein quantification in HEK293T transfected with WT or C4177R-mutant pRNF213 constructs or the pmaxGFP construct (mock control). NT: not transfected. Two-tailed *P* values were determined with unpaired *t*-tests of means ± SD of five independent experiments. **$P \leq 0.01$; ***$P \leq 0.001$.

Figure E1. Skin biopsy. (**A**) Skin biopsy of urticarial lesions from patient (P) 1's back showing a minor infiltrate of small lymphocytes with rare neutrophils (arrowheads) surrounding small capillaries in the upper dermis and scattered nuclear debris interspersed with normal epidermis. (**B**) The infiltrate was predominantly comprised of CD3+ T cells, mixed with CD4+ helper and CD8+ cytotoxic T cells, with scattered FOXP3+ regulatory T cells and cytotoxic effectors (GrzB: Granzyme B, arrowheads). Scale bar: 100 μm.

Figure E2. Laboratory parameters and plasma cytokine measurements. (**A**) P1's and P2's laboratory findings. Abs: antibodies; NA: not available. (**B**) ELISA-assessed plasma-cytokine levels of patients P1 (red circle), P2 (red up-pointing triangle), P3 (red down-pointing triangle) and P4 (red square) and 10 healthy donors (HD) in scatter dot plots with median. (**C**) IL-6 (ELISA) in the supernatants of P1's (n = 2) and P2's (n = 2) and 2 healthy controls' untreated fibroblasts. **A** & **B**: means ± standard deviation.

Figure E3. **Enrichment analyses of differentially expressed genes (DEGs) expressed in patient (P) 1's and 2's monocytes.** (**A**) Top 10 enriched terms listed for up-regulated genes. (**B**) Fold change (FC) of the top 20 up-regulated genes expressed in P1 and P2. Up-regulated genes associated with sepsis are in red. (**C**) Top: Top 10 enriched terms listed for down-regulated genes. Bottom: Heatmap of enriched terms across the list of P1's and P2's down-regulated genes, colored by *P*-values.

Figure E4. Linkage analysis and whole-exome sequencing of patients (P) identifying the *RNF213* c.12529T>C, p.(Cys4177Arg) mutation. (**A**) Linkage-analysis results of 14 family members (8 affected and 6 unaffected) expressed in centimorgans (cM). A genome-wide significant logarithm of the odds (LOD) score was obtained for a single 3.3-Mb region located on chromosome 17 (chr17: 76141133–79461642; hg19 genome assembly). (**B**) P1's and P2's sequence variations identified by whole-exome sequencing and stepwise-elimination process to identify the pathogenic sequence variation. (**C**) The 8 rare P1- and P2-shared variations located in the significant LOD-score chromosome region. (**D**) P1's and P2's exome-sequencing data. Visualization using Integrative Genomics Viewer (IGV) of the *RNF213* c.12529T>C, p.(Cys4177Arg) mutation.

Figure E5. In vitro study of RNF213 transcripts and protein. (**A**) RNF213-mRNA relative expressions in dermal fibroblasts from patient (P) 1's and 2's skin biopsies (SB1 and SB2) and two healthy controls (Ctr). (**B**) Immunoblot analysis of RNF213 and α-tubulin (as loading control) in P1's and P2's SB1 and SB2 dermal fibroblasts and a Ctr. (**C**) Immunoblot analysis of the stability of wild-type (WT) and mutated (C4177R) RNF213 proteins expressed in HEK293T cells and evaluated in the cycloheximide (CHX) assay (100 µg/ml).

Figure E6. RNF213–cell-protein interactions identified by immunoprecipitation (IP) followed by NanoLC MS/MS. (**A**) Venn diagram of proteins interacting with RNF213 in immortalized B cells and in HEK293T cells. (**B**) Immunoblot analysis of RNF213 and CYLD after RNF213 immunoprecipitation (IP) of HEK293T cells transiently expressing the wild-type (WT) or mutated (C4177R) RNF213 protein.

Table E1. RNA-Seq analysis data from P1's and P2's monocytes.

Table E2. Proteomics data from immortalized B cells and HEK293T and obtained after RNF213 immunoprecipitation followed by NanoLC MS/MS.

A

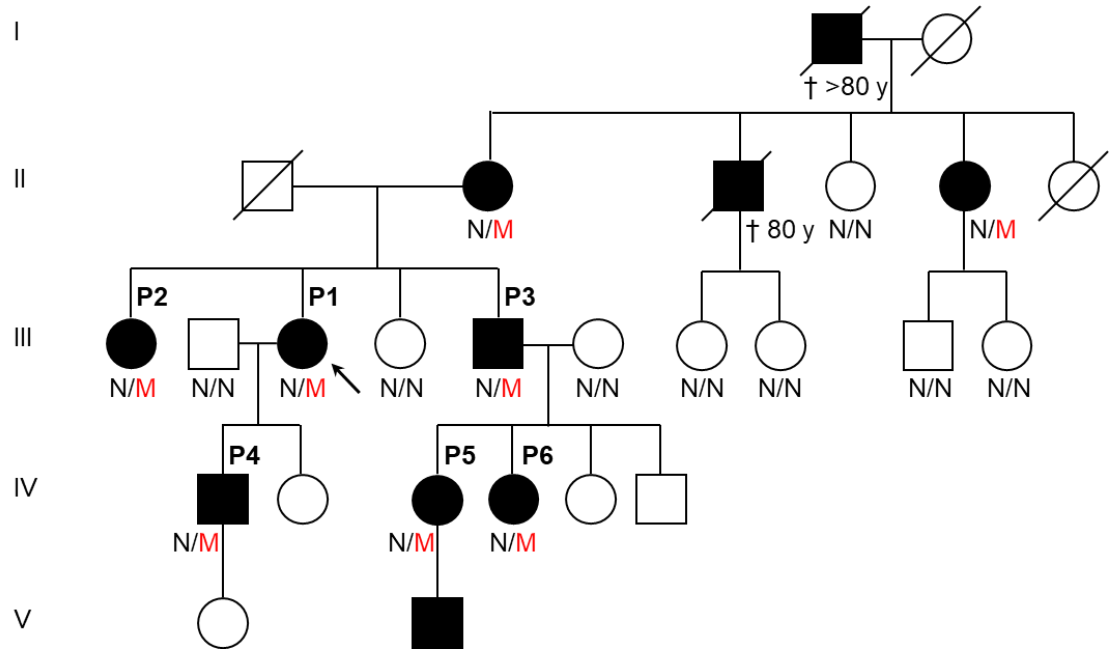

B

P1

P2

C

Patient	P1	P2	P3	P4	P5	P6
Age at onset (years)	12	1	5	0.5	20	14
Age at evaluation (years)	55	56	50	31	27	23
Urticarial lesions	yes	yes	yes	yes	yes	yes
Duration of flares	Continuous, winter aggravation	Several months, winter aggravation	Continuous, winter aggravation	Continuous, winter aggravation	5-7 days, in autumn/winter	2-3 weeks, in winter
Localisation	Face, back, cleavage, arms, legs	Arms, buttock	Back, arms, buttock	Arms, buttock, legs (thighs), ears	Arms, legs (calves, knees)	Back, legs (calves, knees)

Figure 1

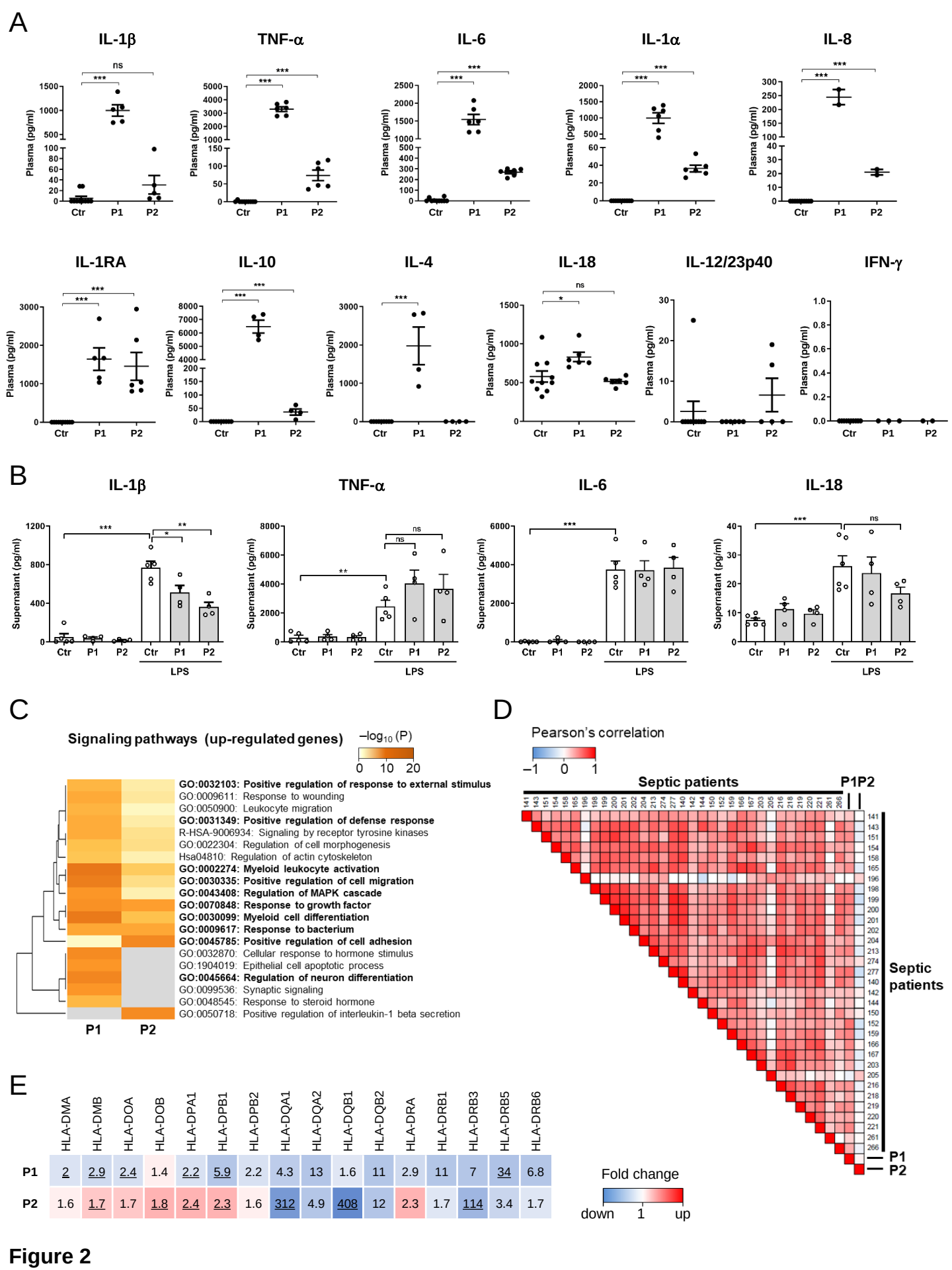
A
IL-1β
TNF-α
IL-6
IL-1α
IL-8
IL-1RA
IL-10
IL-4
IL-18
IL-12/23p40
IFN-γ
Plasma (pg/ml)
Ctr
P1
P2
B
IL-1β
TNF-α
IL-6
IL-18
Supernatant (pg/ml)
LPS
C
Signaling pathways (up-regulated genes)
−log10 (P)
0 10 20
GO:0032103: Positive regulation of response to external stimulus
GO:0009611: Response to wounding
GO:0050900: Leukocyte migration
GO:0031349: Positive regulation of defense response
R-HSA-9006934: Signaling by receptor tyrosine kinases
GO:0022304: Regulation of cell morphogenesis
Hsa04810: Regulation of actin cytoskeleton
GO:0002274: Myeloid leukocyte activation
GO:0030335: Positive regulation of cell migration
GO:0043408: Regulation of MAPK cascade
GO:0070848: Response to growth factor
GO:0030099: Myeloid cell differentiation
GO:0009617: Response to bacterium
GO:0045785: Positive regulation of cell adhesion
GO:0032870: Cellular response to hormone stimulus
GO:1904019: Epithelial cell apoptotic process
GO:0045664: Regulation of neuron differentiation
GO:0099536: Synaptic signaling
GO:0048545: Response to steroid hormone
GO:0050718: Positive regulation of interleukin-1 beta secretion
P1
P2
D
Pearson's correlation
−1 0 1
Septic patients
P1P2
Septic patients
P1
P2
E
HLA-DMA
HLA-DMB
HLA-DOA
HLA-DOB
HLA-DPA1
HLA-DPB1
HLA-DPB2
HLA-DQA1
HLA-DQA2
HLA-DQB1
HLA-DQB2
HLA-DRA
HLA-DRB1
HLA-DRB3
HLA-DRB5
HLA-DRB6
P1 2 2.9 2.4 1.4 2.2 5.9 2.2 4.3 13 1.6 11 2.9 11 7 34 6.8
P2 1.6 1.7 1.7 1.8 2.4 2.3 1.6 312 4.9 408 12 2.3 1.7 114 3.4 1.7
Fold change
down 1 up

Figure 2

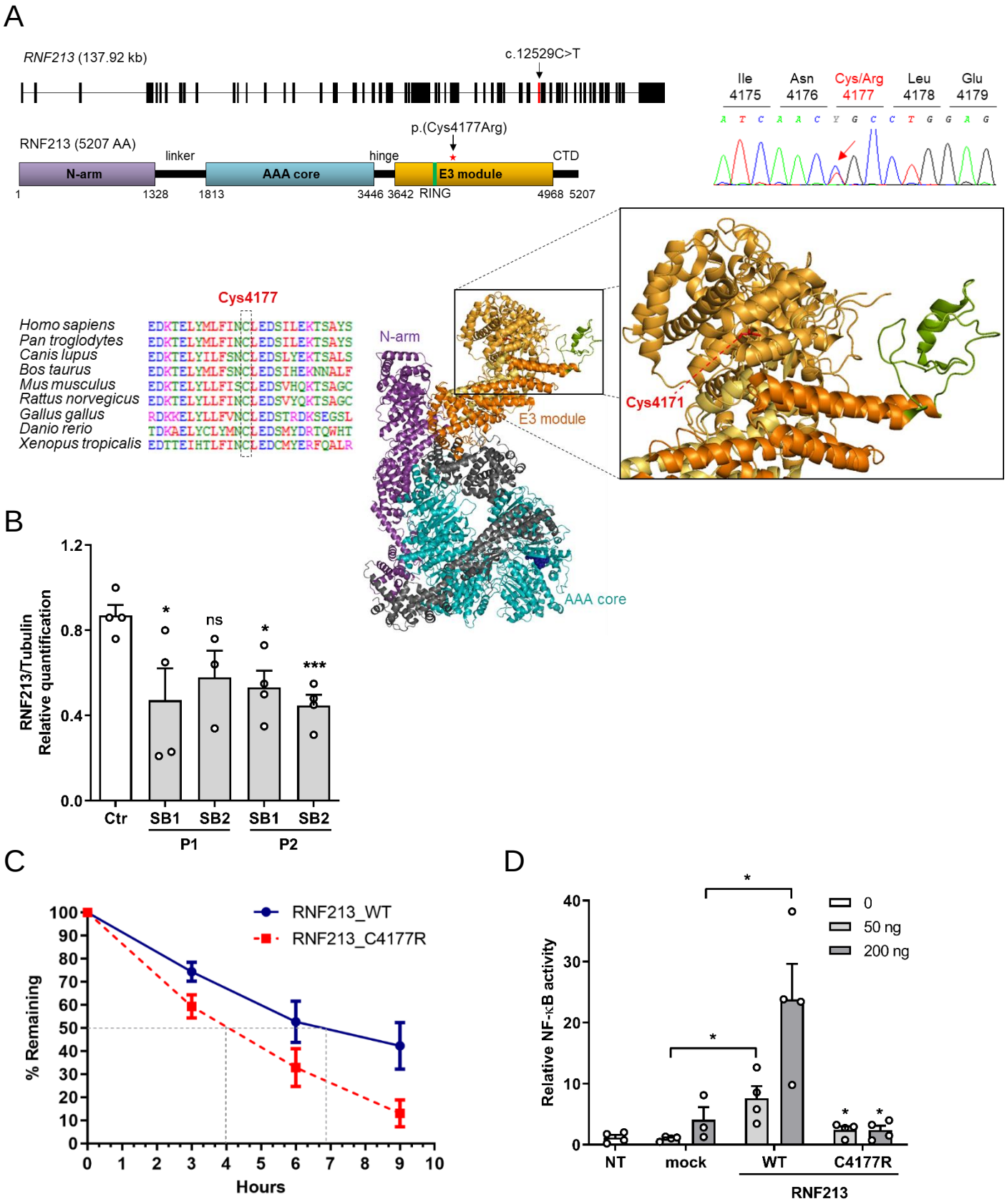
A
RNF213 (137.92 kb)
c.12529C>T
RNF213 (5207 AA)
p.(Cys4177Arg)
linker
hinge
CTD
N-arm
AAA core
E3 module
1
1328
1813
3446 3642
RING
4968 5207
Ile 4175
Asn 4176
Cys/Arg 4177
Leu 4178
Glu 4179
Cys4177
Homo sapiens
Pan troglodytes
Canis lupus
Bos taurus
Mus musculus
Rattus norvegicus
Gallus gallus
Danio rerio
Xenopus tropicalis
N-arm
E3 module
AAA core
Cys4171
B
RNF213/Tubulin
Relative quantification
Ctr
SB1
SB2
SB1
SB2
P1
P2
ns
C
RNF213_WT
RNF213_C4177R
% Remaining
Hours
D
Relative NF-κB activity
0
50 ng
200 ng
NT
mock
WT
C4177R
RNF213

Figure 3

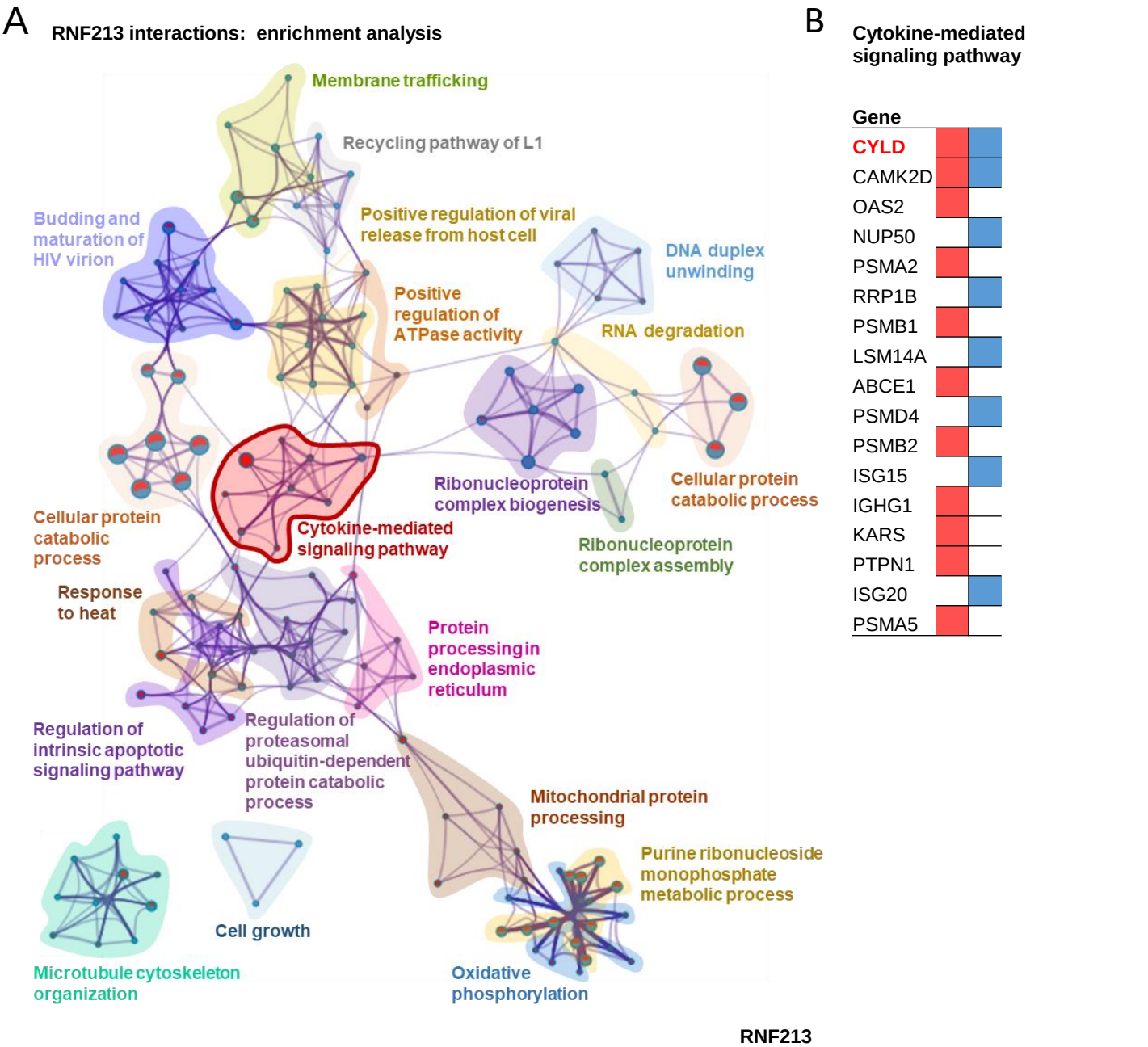
A
RNF213 interactions: enrichment analysis
Membrane trafficking
Recycling pathway of L1
Budding and maturation of HIV virion
Positive regulation of viral release from host cell
DNA duplex unwinding
Positive regulation of ATPase activity
RNA degradation
Ribonucleoprotein complex biogenesis
Cellular protein catabolic process
Cellular protein catabolic process
Cytokine-mediated signaling pathway
Ribonucleoprotein complex assembly
Response to heat
Protein processing in endoplasmic reticulum
Regulation of intrinsic apoptotic signaling pathway
Regulation of proteasomal ubiquitin-dependent protein catabolic process
Mitochondrial protein processing
Purine ribonucleoside monophosphate metabolic process
Cell growth
Microtubule cytoskeleton organization
Oxidative phosphorylation
B
Cytokine-mediated signaling pathway
Gene
CYLD
CAMK2D
OAS2
NUP50
PSMA2
RRP1B
PSMB1
LSM14A
ABCE1
PSMD4
PSMB2
ISG15
IGHG1
KARS
PTPN1
ISG20
PSMA5
C
CYLD/GAPDH
1.0
0.8
0.6
0.4
0.2
0.0
**
***
***
NT
mock
WT
C4177R
RNF213
RNF213
NT
mock
WT
C4177R
250
100
37
RNF213
CYLD
GAPDH

Figure 4

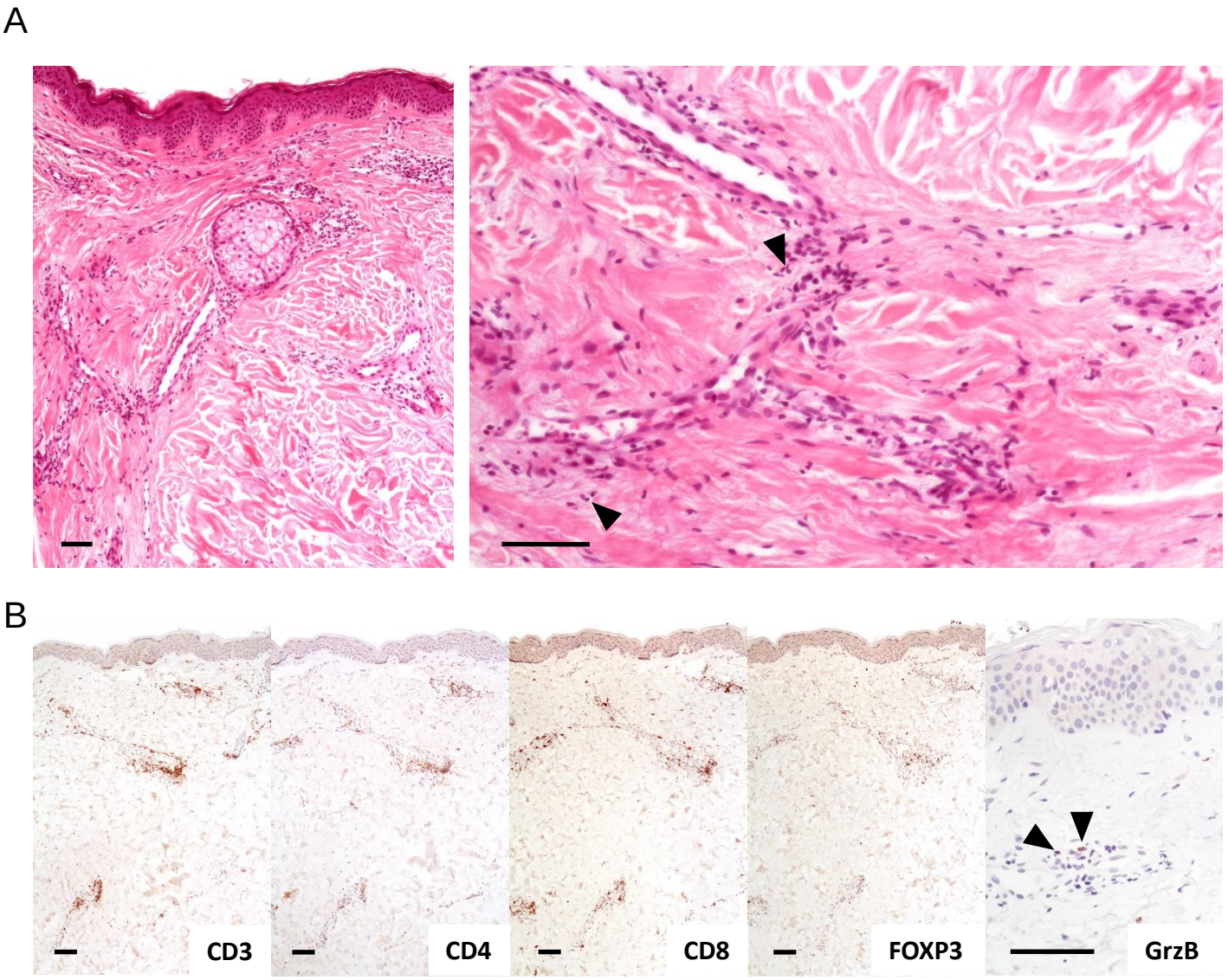

Figure E1

A

	P1	P2	P3	P4	P5	P6	Normal range
Hemoglobin (g/dl)	13.2	13.8	15.8	14.2	12.8	14.0	Females 11.5–17.5 Males 3.0–18.0
Leukocytes (G/l)	3.1	6.4	4.1	3.5	8.4	5.7	4.0–10.0
Platelets (G/l)	231	269	240	293	243	283	150–400
Total lymphocytes (G/l)	**0.6**	2.3	1.2	**0.95**	1.2	2.4	1.0–4.0
CD4+ (cells/µl)	**167**	**1347**	NA	NA	NA	NA	475–1050
CD8+ (cells/µl)	**167**	567	NA	NA	NA	NA	185–570
CD19+ (cells/µl)	79	**226**	NA	NA	NA	NA	50–150
Neutrophils (G/l)	2.0	3.3	2.3	2.2	6.6	2.7	1.5–7.0
Monocytes (G/l)	0.37	0.6	0.5	0.3	0.47	0.48	0.2–1.0
Eosinophils (G/l)	0.069	0.2	0.078	0.11	0.15	0.057	0.02–0.6
Basophils (G/l)	0.050	0	0.029	0.021	0.017	0.052	<0.11
CRP (mg/l)	2.5	2.5	2.2	0.6	2.6	0.9	<5.0
ESR (mm/h)	15	18	**16**	5	9	4	Females <19 Males <11
SAA (mg/l)	**15.6**	**9.4**	**7.7**	<6.4	<6.4	<6.4	<6.4
Total complement – CH50 (U/ml)	57	>60	>60	48	>60	>60	>32
C3 (g/l)	1.20	1.20	1.40	0.90	1.50	1.20	0.90–1.80
C4 (g/l)	0.15	0.22	0.17	0.15	0.17	0.15	0.10–0.40
Ferritin (ng/ml)	**292**	**192**	**1323**	216	22	**152**	Females 15–150 Males 30–400
LDH (U/l)	213	211	229	151	**296**	193	<250
IgA (g/l)	1.33	2.00	**4.29**	2.84	1.70	2.55	0.70–4.00
IgG (g/l)	15.96	13.62	15.53	15.16	12.12	13.98	7.00–16.00
IgM (g/l)	**0.37**	**0.33**	0.42	0.77	0.51	1.54	0.40–2.30
IgD (mg/l)	<13.00	<13.00	30.40	16.10	48.60	38.00	<132.10
IgE (UI/ml)	13.10	66.80	**288.00**	**118.00**	**329.00**	65.10	<114.00
Serum Tryptase (µg/l)	4.8	3.2	3.6	10.7	2.6	1.8	<11.4
Serum Calprotectin (mg/l)	0.62	**0.95**	NA	NA	NA	NA	<0.76
Antinuclear Abs aspect	**320** homogeneous and speckled	**320** homogeneous and speckled	<80	**160** speckled	**80** homogeneous and speckled	<80	<80
dsDNA Abs	Equivocable	Negative	NA	Negative	NA	NA	
ENA Abs panel	Negative	**SSB/La positive**	NA	Negative	NA	NA	

B

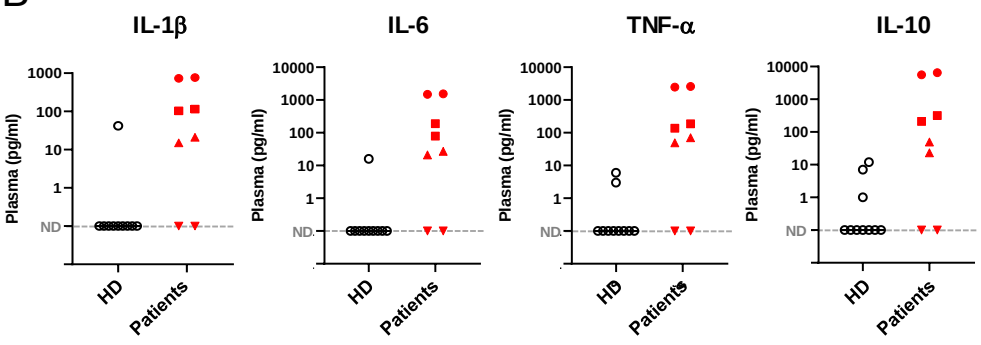

C

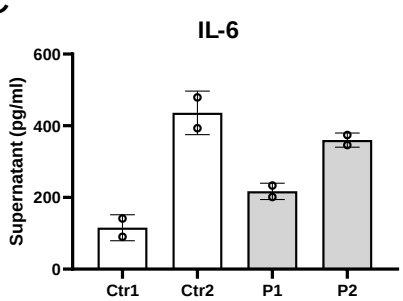

Figure E2

A

Up-regulated genes

Signaling pathways: top 10	Log_{10} (P)
Positive regulation of cell migration	–9.83
Myeloid leukocyte activation	–9.17
Response to bacterium	–9.16
Myeloid cell differentiation	–9.16
Response to growth factor	–8.70
Positive regulation of response to external stimulus	–7.69
Positive regulation of defense response	–7.54
Regulation of MAPK cascade	–7.47
Regulation of neuron differentiation	–7.32
Positive regulation of cell adhesion	–7.13

B

Up-regulated genes

P1		P2	
Gene	**FC**	**Gene**	**FC**
OLFM4	263.09	*CLLU1OS*	341.67
LINC02470	90.44	*TREML4*	74.44
TREML4	77.43	*HSPB7*	39.3
RETN	21.17	*BIRC7*	29.16
CEACAM8	14.27	*HTRA3*	18.84
CD177	13.55	*ULBP2*	11.3
BPI	11.32	*ADGRG1*	10.55
ANXA3	10.82	*CX3CR1*	9.85
LCN2	9.96	*NME8*	9.42
IL6	9.52	*S100B*	9.05
STON2	9.12	*GAL*	8.38
PGLYRP1	8.74	*LGR6*	8.31
LTF	8.38	*SLC22A23*	8.21
GPRC5D-AS1	7.83	*GPRC5D-AS1*	8.2
HSPB7	7.83	*CHIT1*	7.91
CAMP	7.08	*GALNT14*	7.61
HPGD	6.79	*FCRL6*	7.53
GAL	6.76	*TLN2*	7.4
MMP8	6.65	*NRIR*	7.17
ARG1	6.65	*MYEOV*	6.99

C

Down-regulated genes

Signaling pathways: top 10	Log_{10} (P)
Ribosome, cytoplasmic	–59.55
T-cell activation	–23.27
Hematopoietic cell lineage	–12.83
Adaptive immune response	–12.49
Alpha–beta T-cell activation	–11.20
T-cell selection	–9.27
Antigen receptor-mediated signaling pathway	–8.65
Ribosome assembly	–8.49
Leukocyte migration	–7.45
Lymphocyte costimulation	–6.53

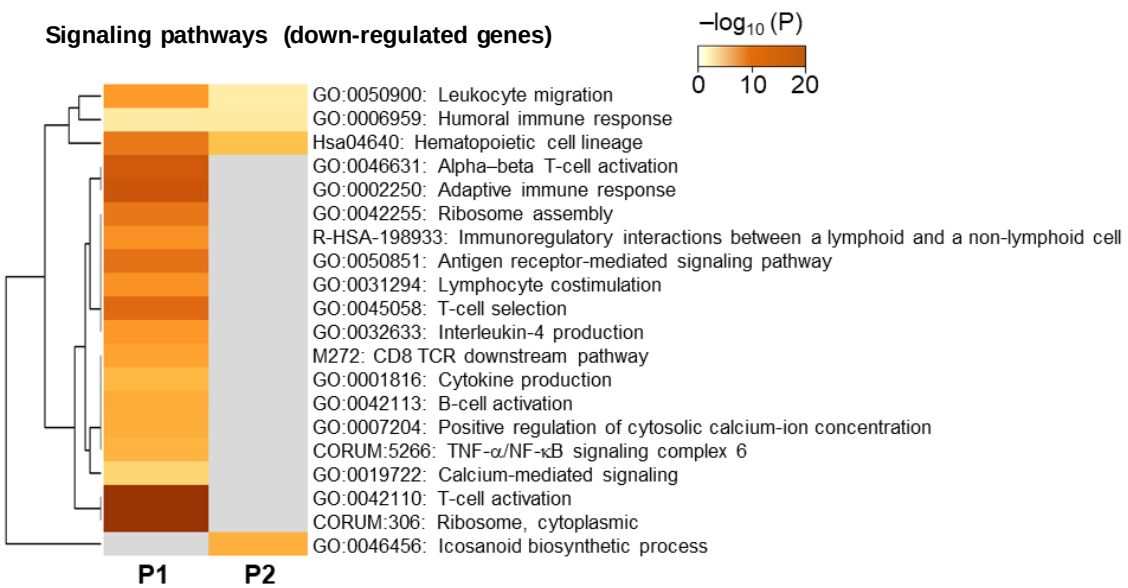

Figure E3

A

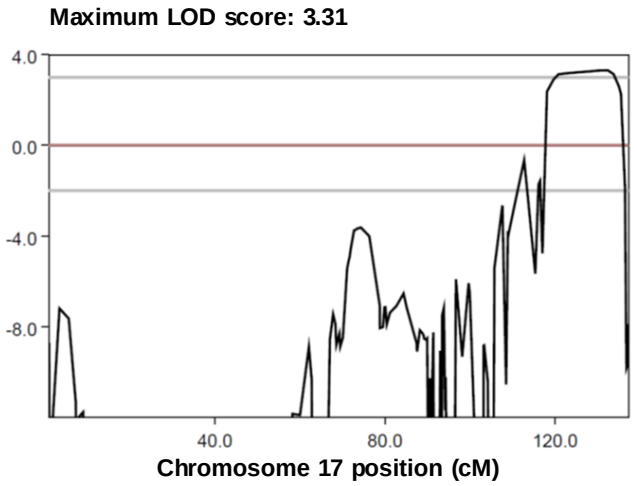

B

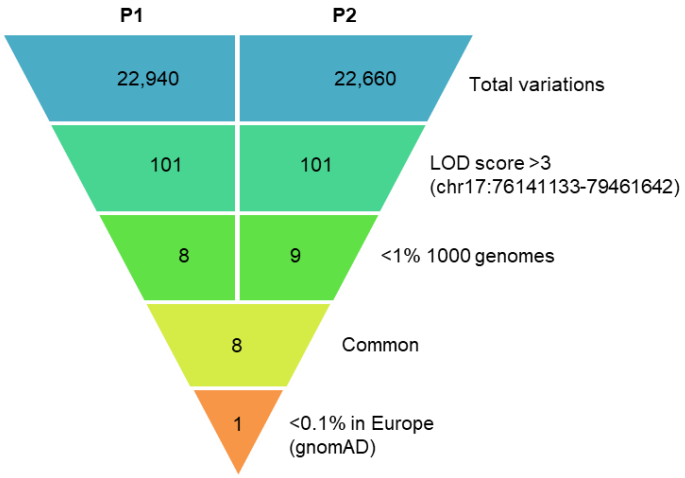

C

Variation	Genotype	gnomAD	gnomAD Europe
DNAH17 (NM_173628) Exon 42, c.6462C>T p.(Ala2154Ala)	heterozygous	1718/278058	1293/127052 (1.02%)
DNAH17 (NM_173628) Exon 26, c.4042C>T p.(Arg1348Cys)	heterozygous	573/280614	498/128386 (0.39%)
USP36 (NM_025090) Exon 4, c.318C>A p.(Pro106Pro)	heterozygous	3117/282174	1878/128830 (1.46%)
GAA (NM_000152) Exon 4, c.858+5insGCAGCGG	homozygous	181917/274012 †	90918/123654 (73.5%)
***RNF213* (NM_001256071) Exon 47, c.12529T>C p.(Cys4177Arg)**	**heterozygous**	**0**	**0**
ENTHD2 (NM_144679) Exon 6, c.437G>T p.(Gly146Val)	heterozygous	2043/256456	1399/117278 (1.19%)
SLC38A10 (NM_138570) Exon 14, c.2284_*1del	heterozygous	9488/241908	3049/114298 (2.67%)
SLC38A10 (NM_001037984) Exon 11, c.1146C>T p.(Val382Val)	heterozygous	2385/275134	1514/124790 (1.21%)

† Frequent variation (different annotations).

D

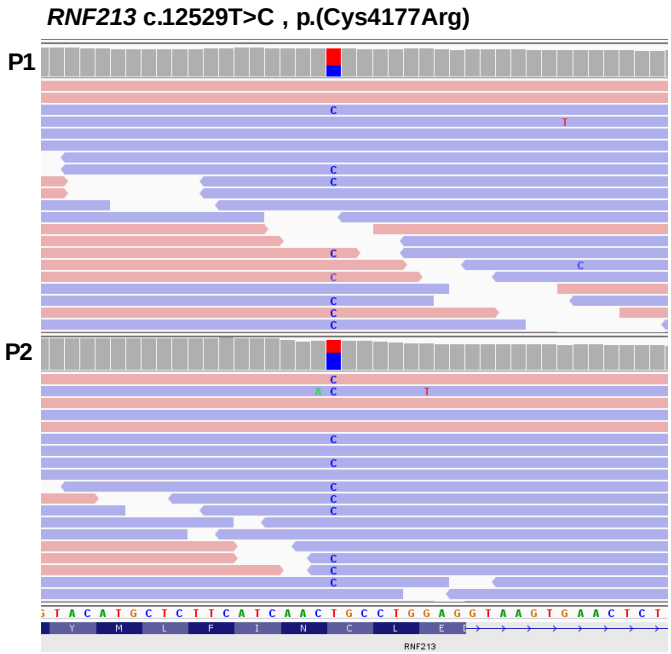

Figure E4

A

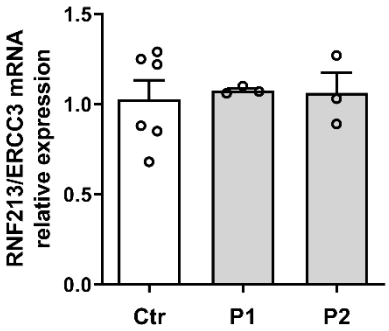

B

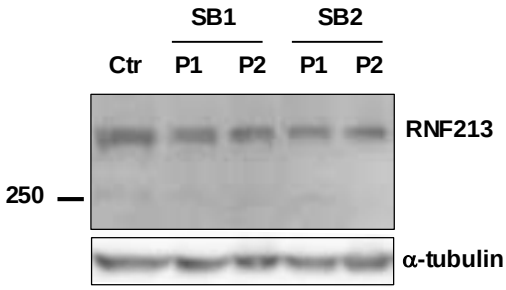

C

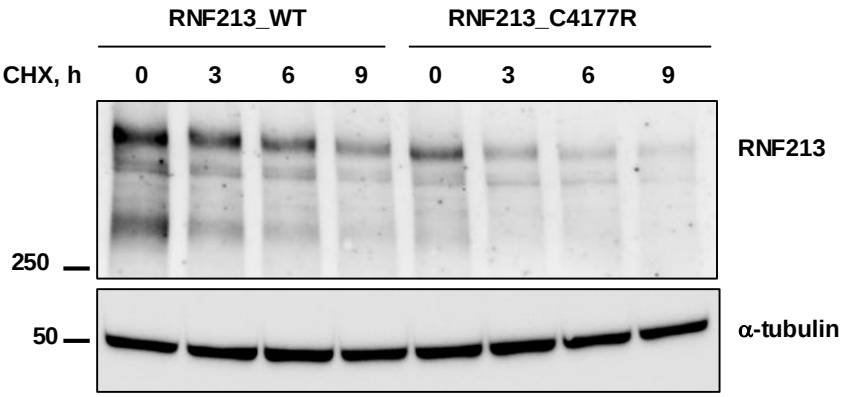

Figure E5

A

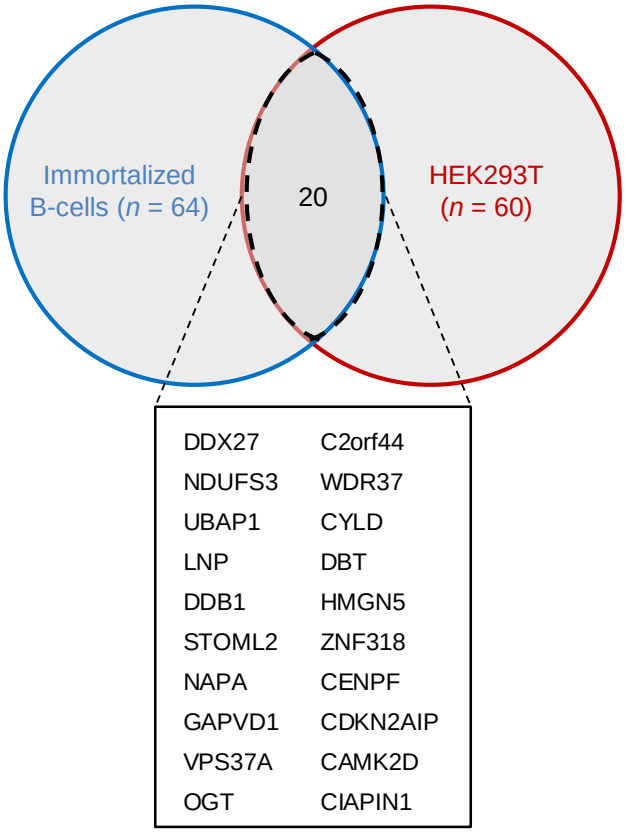
RNF213 interactions
Immortalized
B-cells (n = 64)
20
HEK293T
(n = 60)
DDX27
NDUFS3
UBAP1
LNP
DDB1
STOML2
NAPA
GAPVD1
VPS37A
OGT
C2orf44
WDR37
CYLD
DBT
HMGN5
ZNF318
CENPF
CDKN2AIP
CAMK2D
CIAPIN1

B

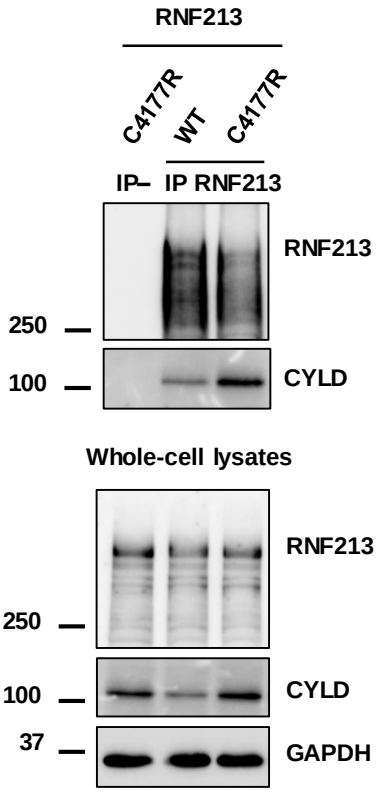
RNF213
C4177R
WT
C4177R
IP–
IP RNF213
RNF213
250
100
CYLD
Whole-cell lysates
RNF213
250
100
CYLD
37
GAPDH

Figure E6